Shear Strength of Fractures in Phu Kradung Sandstone Under True Triaxial Stresses

Piyanat Kapang and Kittitep Fuenkajorn

School of Geotechnology, Institute of Engineering, Suranaree University of Technology,

Muang District, Nakhon Ratchasima, Thailand 30000.

Phone (66-44) 224-758, Fax (66-44) 224-448

E-Mail: kittitep@sut.ac.th

Abstract

True triaxial shear tests have been performed to determine the peak shear strengths of tension-induced fractures in Phu Kradung sandstone. A polyaxial load frame is used to apply mutually perpendicular lateral stresses (σ_p and σ_o) to the 76×76×126 mm rectangular block specimens. The normal of the fracture plane makes an angle of 59.1° with the axial (major principal) stress. Results indicate that the lateral stress that is parallel to the fracture plane (σ_p) can significantly reduce the peak shear strength of the fractures. Under the same normal stress (σ_n) the fractures under high σ_p dilate more than those under low σ_p. According to the Coulomb criterion, the friction angle decreases with increasing σ_p/σ_o ratio and the cohesion decreases with increasing σ_p. The lateral stress σ_p has insignificant effect on the basic friction angle of the smooth saw-cut surfaces. The fracture shear strengths under σ_p = 0 correlate well with those obtained from the direct shear tests. It is postulated that when the fractures are laterally confined by σ_p, their asperities are strained into the aperture, and are sheared off easier compared to those under unconfined condition.

1. Introduction

Direct shear testing [1] has widely been used to determine the peak and residual strengths of the rock fractures. Its test configurations however pose some disadvantages that the magnitudes of the applied normal stress are limited by the uniaxial compressive strength of the rock and that the fractures are sheared under unconfined conditions. The triaxial shear testing [2-3] has been developed to simulate the frictional resistance of rock fractures under confinements. The cylindrical rock core containing an inclined fracture or weakness plane can be axially loaded in a triaxial pressure cell with a wide range of applied confining pressures. The normal stress at which the shear strengths are measured can be controlled by the applied axial stress and confining pressures. Determination of the fracture shear strengths under true triaxial stresses where the shear sliding occurs under anisotropic stresses ($\sigma_1 \neq \sigma_2 \neq \sigma_3$) has not been attempted.

The objective of this study is to experimentally determine the shearing resistance of fractures in sandstone specimens under true triaxial stresses. The effort involves performing true triaxial shear tests on tension-induced fractures and smooth saw-cut surfaces by using a polyaxial load frame. The conventional direct shear tests are also performed to compare their results with those of the true triaxial stresses.

2. Sample Preparation

The specimens used for the true triaxial shear tests are prepared from the Phu Kradung sandstone (hereafter designated as PKSS). They are cut to obtain rectangular blocks with nominal dimensions of 76×76×126 mm^3. The rock is classified as fine-grained quartz sandstones with highly uniform texture and density. A line load is applied to

RECEIVED 25 July, 2012

ACCEPTED 20 November, 2012

obtain a tension-induced fracture diagonally across the sandstone block, as shown in Figure 1. The normal to the fracture plane makes an angle of 59.1° with the major axis of the specimen. All fractures are clean and well mated. The asperity amplitudes on the fracture planes are measured from the laser-scanned profiles along the shear direction. The readings are made to the nearest 0.01 mm. The maximum amplitudes are used to estimate the joint roughness coefficients (JRC) of each fracture based on Barton's chart [4]. The joint roughness coefficients are averaged as 6-8. All specimens are oven-dried before testing. For the direct shear test specimens a line load is applied to obtain a tension-induced fracture at the mid-section of the 100×100×160 mm^3 sandstone blocks. The fracture area is 100×100 mm^2.

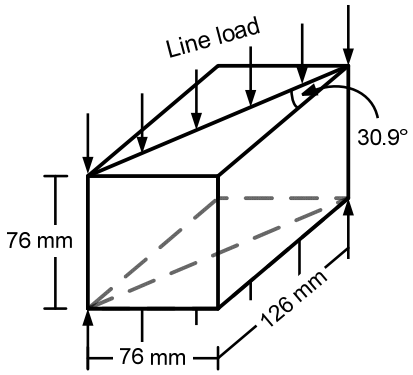

Figure 1 Line load applied to obtain tension-induced fracture in sandstone specimen.

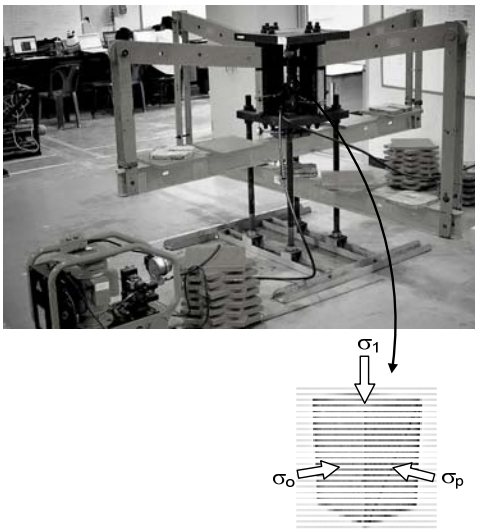

Figure 2 Polyaxial load frame used in this study.

3. Polyaxial Load Frame

A polyaxial load frame [5] is used to apply true triaxial stresses to the specimens (Figure 2). One of the lateral stresses is parallel to the fracture plane which is designated as σ_p. The other is on the fracture plane and is designated as σ_o. They are applied by two pairs of 152 cm long cantilever beams set in mutually perpendicular directions. The outer end of each beam is pulled down by a dead weight placed on a lower steel bar linking the two opposite beams underneath. The beam inner end is hinged by a pin mounted between vertical bars on each side of the frame. During testing all beams are arranged nearly horizontally, and hence a lateral compressive load results on the specimen placed at the center of the frame. Using different distances from the pin to the outer weighting point and to the inner loading point, a load magnification of 11 to 1 is obtained. This loading ratio is also used to determine the lateral deformation of the specimen by monitoring the vertical movement of the two steel bars below. Prior to testing the lateral loads are calibrated to obtain the desired lateral stresses using an electronic load cell.

4. Test Procedure

The sandstone specimen is installed into the load frame with neoprene sheets placed at all interfaces between loading platens and rock surfaces to minimize the friction. Dead weights are placed on the two lower bars to obtain the pre-defined magnitude of the lateral stresses (σ_o and σ_p) on the specimen. Simultaneously the axial (vertical) stress is increased to the same value with σ_o to obtain the condition where both shear and normal stresses are zero on the fracture plane. This is set as an initial stress condition. The test is started by increasing the axial stress

at a constant rate using the electric oil pump while σ_p and σ_o are maintained constant. The specimen deformations in the three loading directions are monitored. The readings are recorded every 10 kN of the axial load increment until the peak shear stress is reached. Figure 3 shows the directions of the applied stresses with respect to the fracture orientation. It is assumed here that the sliding direction is on the σ_1-σ_o plane, i.e., perpendicular to the σ_p axis. As a result the shear stress (τ) and its corresponding normal stress (σ_n) increase with σ_1, which can be determined as follows:

$$\tau = \frac{1}{2}(\sigma_1 - \sigma_o)\sin 2\beta \quad (1)$$

$$\sigma_n = \frac{1}{2}(\sigma_1 + \sigma_o) + \frac{1}{2}(\sigma_1 - \sigma_o)\cos 2\beta \quad (2)$$

where σ_1 and σ_o are the axial and lateral stresses, and β is the angle between σ_1 and σ_n directions. For all specimens the angle β equals to 59.1 degrees.

The effect of the friction at the interfaces between the steel platen and the lateral neoprene sheet is measured by vertically loading an intact sandstone block with the same dimensions as used above while the constant lateral stresses are applied. A linear relationship between the axial resistance and the applied lateral stresses are obtained as shown in Figure 4. The results are used to correct the magnitudes of the axial stress measured during the fracture shearing tests.

Four test series are performed as follows:

(1) true triaxial shear tests of tension-induced fractures under constant σ_p/σ_o ratio,

(2) true triaxial shear tests of tension-induced fractures under constant σ_p,

(3) true triaxial shear tests of smooth surfaces under constant σ_p, and

(4) direct shear tests of tension-induced fractures.

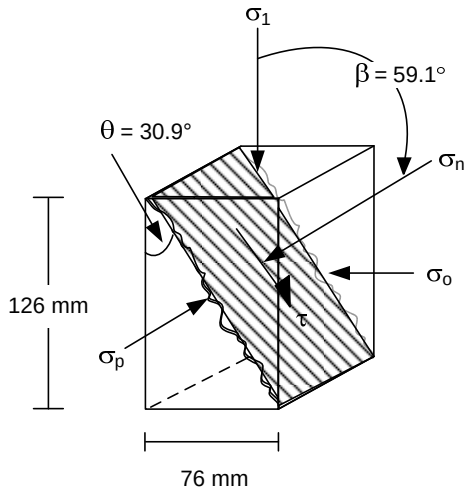

Figure 3 Shear (τ) and normal (σ_n) stresses calculated from the applied axial stress (σ_1) and lateral stress on the fracture plane (σ_o).

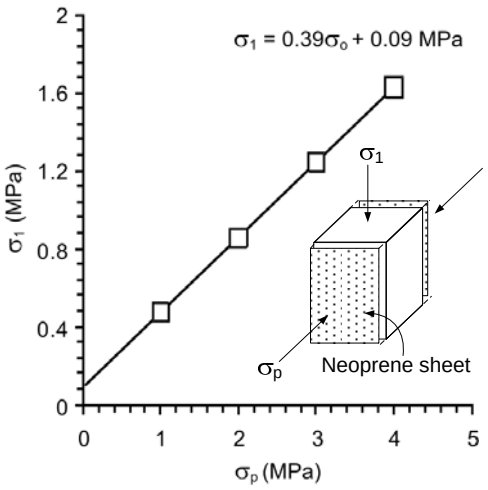

Figure 4 Axial resistance between loading platens and neoprene sheets induced by lateral stress (σ_p).

5. Shear Strength of Fractures Under Constant σ_p/σ_o Ratio

For this test series the peak shear strengths are determined for the lateral stress ratios (σ_p/σ_o) of 0, 0.5, 1, 2, 3 and 4. A minimum of four specimens are tested for each lateral stress ratio. The conditions where σ_p/σ_o is 0 and 1 are equivalent to the direct shear testing and the triaxial shear testing. Table 1 summarizes the shear strength results. Examples of the

Table 1 Peak shear strength for σ_p/σ_o = 0, 0.5, 1, 2, 3 and 4 MPa.

σ_p/σ_o	σ_p (MPa)	σ_o (MPa)	σ_1 (MPa)	σ_n (MPa)	τ (MPa)
0	0	0.6	14.83	4.16	6.16
	0	1	18.01	5.25	7.37
	0	2	24.21	7.55	9.62
	0	2.5	26.61	8.53	10.44
	0	3	30.26	9.81	11.83
	0	3.5	34.90	11.35	13.59
	0	4	36.43	12.11	14.04
	0	4.5	41.01	13.63	15.81
	0	5	42.54	14.38	16.25
0.5	1	2	17.53	5.88	6.73
	1.5	3	22.00	7.75	8.23
	2	4	27.14	9.79	10.02
	3	6	32.20	12.55	11.35
1	0.6	0.6	7.69	2.37	3.07
	1	1	8.98	3.00	3.46
	2	2	11.92	4.48	4.30
	3	3	15.94	6.24	5.60
	4	4	18.11	7.52	6.11
	5	5	21.72	9.18	7.24
	7	7	25.15	11.54	7.86
2	2	1	7.91	2.73	2.99
	4	2	10.23	4.05	3.56
	6	3	12.38	5.35	4.06
	8	4	14.80	6.70	4.67
	10	5	18.66	8.41	5.91
3	3	1	7.85	2.71	2.97
	6	2	10.02	4.00	3.47
	9	3	11.22	5.06	3.56
	12	4	13.24	6.31	4.00
4	4	1	7.43	2.61	2.79
	8	2	9.03	3.76	3.04
	12	3	10.12	4.78	3.08
	16	4	11.11	5.78	3.08

shear stress-displacement (τ-d_s) curves for some specimens shown in Figure 5. The shear and normal displacements (d_s and d_n) are calculated by:

$$d_s = \frac{1}{2}(d_1 - d_o)\sin 2\beta \quad (3)$$

$$d_n = \frac{1}{2}(d_1 + d_o) + \frac{1}{2}(d_1 - d_o)\cos 2\beta \quad (4)$$

where d_1 and d_o are the specimen displacements monitored in the directions of σ_1 (axial) and σ_o during the test.

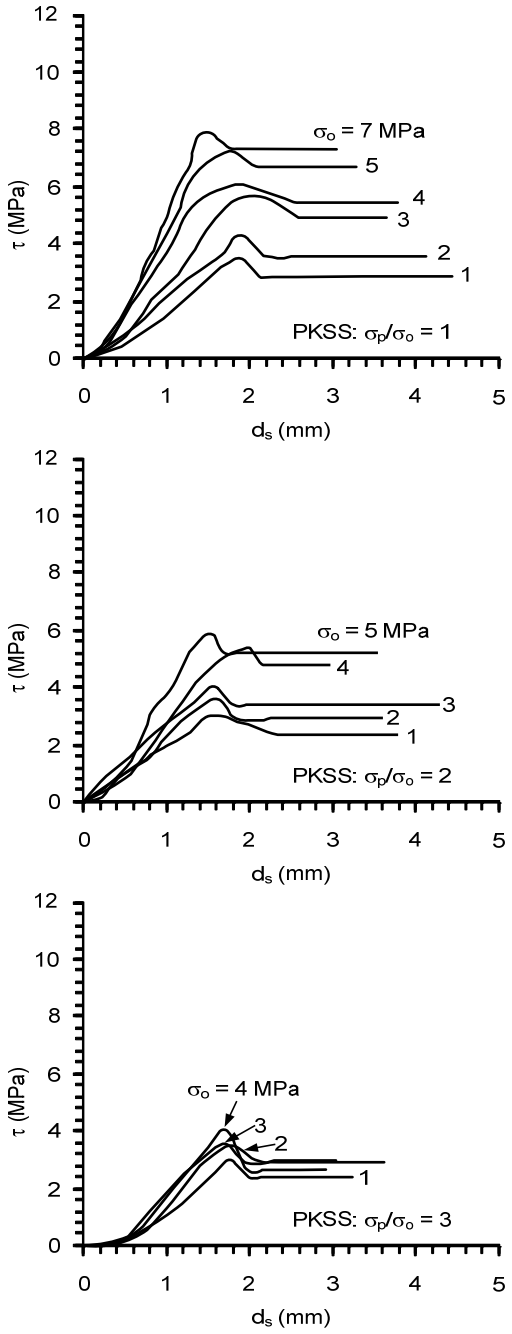

Figure 5 Shear stresses (τ) as a function of shear displacement (d_s) for some σ_p/σ_o ratios.

Figure 6 shows the fracture dilation (normal displacement) as a function of the shear displacement monitored during the test.

Based on the Coulomb criterion a linear relation is proposed to represent the peak shear strengths under various σ_p/σ_o ratios as follows:

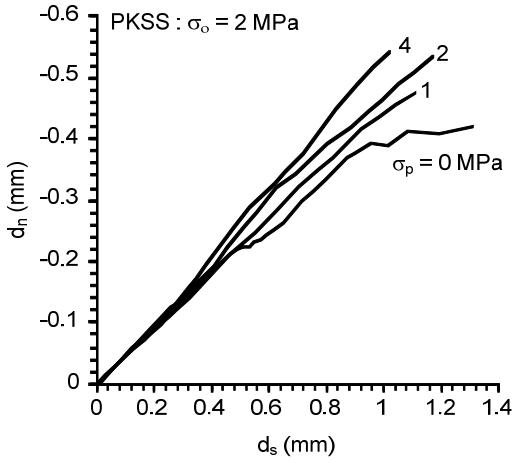

Figure 6 Normal displacement as a function of shear displacement for some specimens.

$$\tau = \sigma_n \tan(\phi^*) + c^* \quad (5)$$

where ϕ^* and c* are defined here as the apparent friction angle and apparent cohesion of the fractures. This is primarily to avoid confusing with the fracture cohesion (c) and friction angle (ϕ) conventionally obtained from the direct shear test with constant normal stress The above equation is fitted to the experimental results in the forms of τ-σ_n diagram in Figure 7. The apparent friction angle decreases with increasing lateral stress ratios (σ_p/σ_o), which can be best described by an exponential equation (Figure 8):

$$\phi^* = \alpha \exp\left[-\kappa\left(\frac{\sigma_p}{\sigma_o}\right)\right] \quad (6)$$

where α and κ are empirical constants. Their numerical values are given in Figure 8.

The apparent cohesions obtained from this test series tend to be independent of σ_p/σ_o ratio. They are averaged as 2.18. Post-test observations show that the sheared off areas for the fractures under higher lateral stress σ_p tend to be larger than those tested under lower σ_p. Figure 9 shows some post-test specimens.

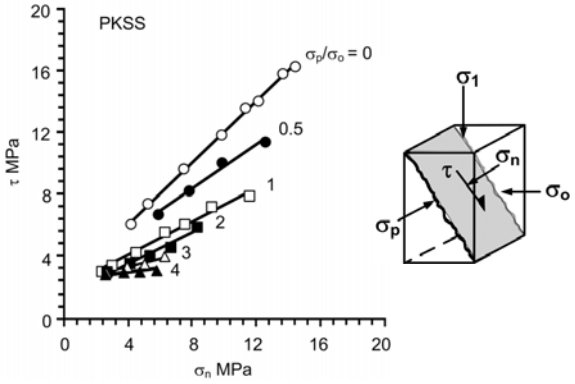

σ_p/σ_o	$\tau = \sigma_n \tan\phi^* + c^*$		R^2
(MPa)	ϕ^* (Degrees)	c* (MPa)	
0	45	2.01	0
0.5	35	2.77	0.5
1	29	1.91	1
2	27	1.51	2
3	15	2.27	3
4	5	2.62	4

Figure 7 Peak shear strength (τ) as a function of normal stress (σ_n).

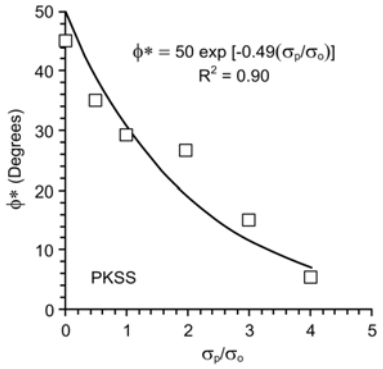

Figure 8 Apparent friction angles (ϕ^*) as a function of σ_p/σ_o ratio.

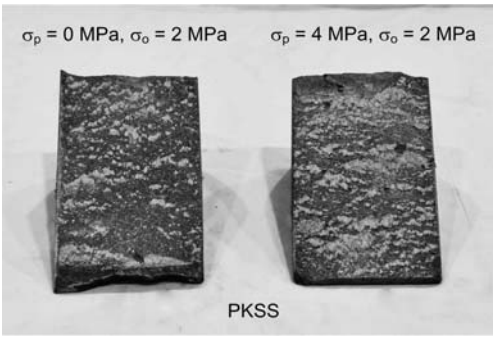

Figure 9 Some post-test fracture surfaces.

6. Shear Strength of Fractures Under Constant σ_p

The configurations of the sandstone specimens and test procedure for this test series are identical to those mentioned above. Here σ_p is maintained constant at 1, 2 and 3 MPa while σ_o is varied from 1.5 to 6 MPa. Table 2 summarized the strength results. They are presented in the forms of τ-σ_n diagram in Figure 10. For a comparison the true triaxial testing results at σ_p=0 are also incorporated into the figure. It is found that the lateral stress σ_p can notably decrease the fracture shear strengths. A linear relation between the peak shear strengths and the normal stresses is obtained at all levels of σ_p which can also be represented by equation (5), as shown in Figure 13. In this diagram ϕ* tends to be independent of σ_p while c* decreases exponentially as σ_p increases. The c*- σ_p relation can be represented by:

$$c^* = \psi \exp\left[-\xi\left(\sigma_p\right)\right] \quad (7)$$

where ψ and ξ are empirical constants. Their numerical values obtained from regression analysis are given in Figure 11. The apparent friction angles from the constant σ_p tests are averaged as 44°.

By substituting equations (6) and (7) into (5) the following relation is obtained.

$$\tau = \sigma_n \tan\left\{\alpha \exp\left[-\kappa\left(\frac{\sigma_p}{\sigma_o}\right)\right]\right\} + \psi \exp\left[-\xi\left(\sigma_p\right)\right] \quad (8)$$

7. Shear Strength of Smooth Surfaces Under Constant σ_p

This test series is performed to determine the σ_p effect on the shearing resistance of the smooth saw-cut surfaces. The test method and strength calculation are identical to those of the tension-induced fractures. The σ_p values are maintained constant at 1, 2 and 3 MPa, and the lateral stress σ_o varies from 2 to 10 MPa. Figure 12 shows the test results in the

Table 2 Triaxial shear strengths with constant σ_p at 1, 2 and 3 MPa.

σ_p (MPa)	σ_o (MPa)	σ_1 (MPa)	σ_n (MPa)	τ (MPa)
1	1.5	14.52	4.75	5.64
	2	17.53	5.88	6.73
	2.5	22.17	7.41	8.52
	3	25.25	8.56	9.63
	3.5	27.86	9.59	10.55
	4	31.35	10.84	11.84
	4.5	34.41	11.98	12.95
	5	36.86	12.97	13.80
2	2.5	17.14	6.16	6.34
	3	20.34	7.33	7.51
	3.5	23.34	8.46	8.59
	4	27.14	9.79	10.02
	4.5	29.39	10.72	10.77
	5	31.45	11.61	11.45
3	4	22.08	8.52	7.83
	4.5	25.11	9.65	8.93
	5	27.50	10.63	9.74
	5.5	29.61	11.53	10.44
	6	32.20	12.55	11.35

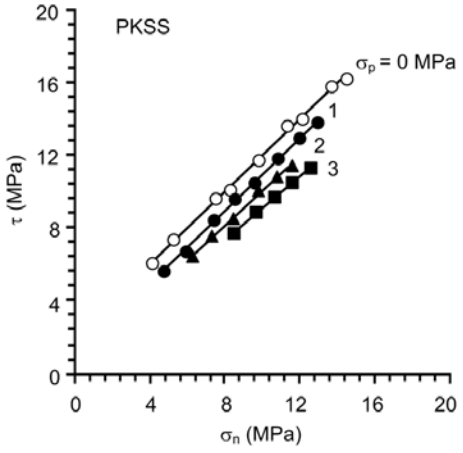

σ_p (MPa)	$\tau = \sigma_n \tan\phi^* + c^*$		R^2
	ϕ^* (Degrees)	c* (MPa)	
0	45	2.00	0.99
1	45	0.95	0.99
2	44	0.53	0.99
3	42	0.54	0.99
$\phi^*_{average}$ = 44.0 Degrees			

Figure 10 Peak shear strength (τ) as a function of normal stress (σ_n).

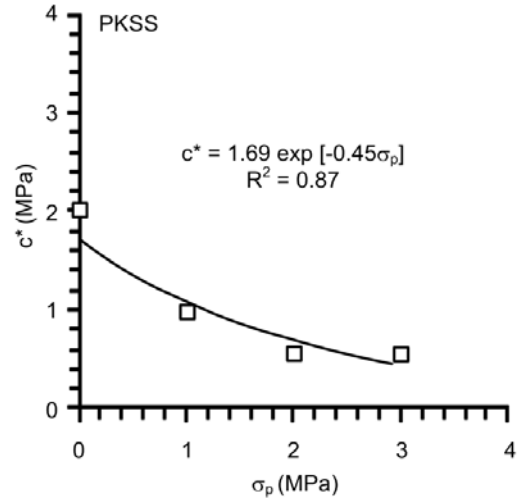

Figure 11 Apparent cohesion (ϕ*) as a function of σ_p.

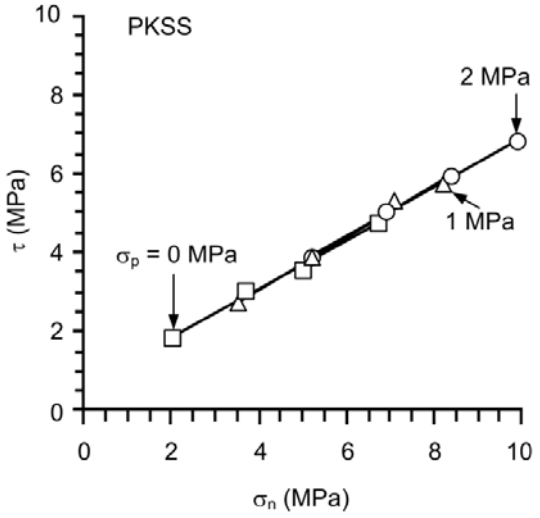

σ_p (MPa)	$\tau = \sigma_n \tan\phi^* + c^*$		R^2
	ϕ^* (Degrees)	c* (MPa)	
0	31	0.69	0.99
1	33	0.45	0.97
2	32	0.70	0.99
$\phi^*_{average}$ = 32 Degrees		$c^*_{average}$ = 0.61 MPa	

Figure 12 Shear strengths of smooth saw-cut surfaces.

forms of τ-σ_n diagram where they are correlated well with the linear relation given by equation (5). The shearing resistances for the smooth surfaces of the three tested sandstones tend to be independent of the lateral stress σ_p, as evidenced by the similar values of ϕ*and c* obtained from different magnitudes of σ_p. This indicates that the load correction for the frictional resistance (induced by σ_p) at the platen-neoprene interfaces is appropriate.

8. Direct Shear Tests

The direct shear tests are performed on the tension-induced fractures to verify the reliability of the true triaxial test results above and to correlate the fracture shear strengths obtained from the two tests. The stress paths used for the two shear tests are different. For the true triaxial shear test both normal and shear stresses increase with the applied axial stress. For the direct shear test the normal stress is maintained constant during shearing (i.e. constant normal load test – CNL).

Figure 13 shows the shear stresses and normal displacements as a function of shear displacement for all specimens. The direct shear strengths are compared with the true triaxial shear strengths under $\sigma_p = 0$ in Figure 14. Based on the Coulomb criterion both tests show similar cohesions and friction angles. Some discrepancies may be due to the intrinsic variability of the rock fractures. The results suggest also that under the range of the normal stresses used here different stress paths have insignificant impact on the peak shear strengths of the tension-induced fractures of the three sandstones.

Let assume here that the peak shear strengths from both tests are the same for the condition where $\sigma_p = 0$, equations (6), (7) and (8) reduce to

$$\phi^* = \alpha \tag{9}$$

$$c^* = \psi \tag{10}$$

$$\tau = \sigma_n \tan\alpha + \psi \tag{11}$$

Under unconfined condition the parameters α and ψ become the friction angle (ϕ) and cohesion (c) of the fracture. An alternative form of equation (8) can therefore be written as:

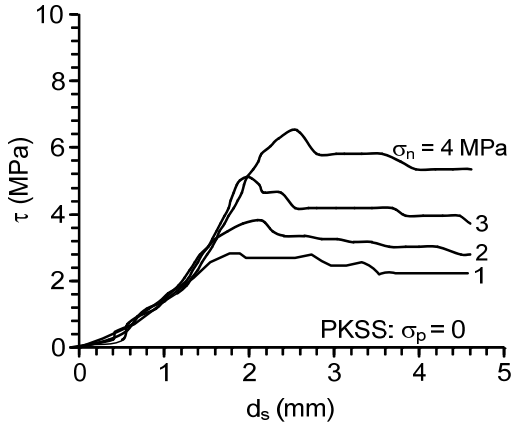

Figure 13 Direct shear test results.

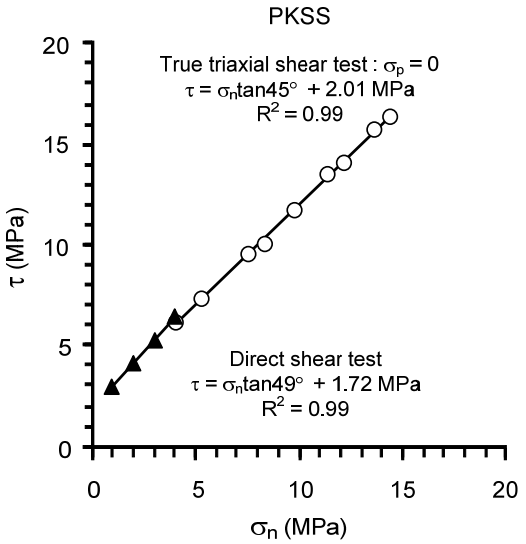

Figure 14 Direct shear tests results compared with true triaxial shear test results at $\sigma_p = 0$.

$$\tau = \sigma_n \tan\left\{\phi \cdot \exp\left[-\kappa\left(\frac{\sigma_p}{\sigma_o}\right)\right]\right\} + c \cdot \exp\left[-\xi\left(\sigma_p\right)\right] \quad (12)$$

Equation (12) allows a transition of the fracture shear strengths from the unconfined condition ($\sigma_p = 0$, direct shear testing) to the confined conditions ($\sigma_p > 0$, true triaxial shear testing).

9. Discussions and Conclusions

The results from this study can be concluded that the lateral stress (σ_p) that is parallel to the sliding plane and perpendicular to the sliding direction can significantly reduce the magnitudes of the cohesion and friction angle of the fractures. The greater magnitudes of the lateral stress σ_p will result in the larger sheared off areas and the larger dilations. This means that application of the fracture shear strengths from the direct shear testing may not be conservative when the fractures are subject to multi-axial stresses under in-situ conditions.

It is postulated that σ_p induces lateral tensile strains (dilation) of the rock asperities into the fracture aperture. These asperities can be sheared off more easily when the fractures subject to shear load, and hence resulting in a lower frictional resistance. This is evidenced by that σ_p has no effect on the shear strength of smooth saw-cut surfaces. This implies that the reduction of the cohesion and friction angle also depends on the roughness characteristics (amplitudes, scale, and asperity strength). For fractures in other rocks that have different surface roughness and strengths from those tested here they may exhibit different behavior and degrees of the σ_p-dependent shear strengths. Different shear strength criteria may be required to describe the results if the τ-σ_n diagram is non-linear. Different empirical forms may also be a better alternative for the relations between the apparent friction angle and the lateral stress ratio (σ_p/σ_o) and between the apparent cohesion and the lateral stress σ_p.

The exponential form used here has an advantage that it allows a transition of the shear strengths under the unconfined condition (e.g., direct shear testing) to under the true triaxial stress states. The proposed relation is supported by that the test results from the direct shear testing and from the true triaxial shear testing under $\sigma_p = 0$ are very similar. This suggests that the loading path has insignificant impact on fracture shear strengths of the tested sandstone. Care should be taken to apply the findings above to the actual

in-situ conditions due the relatively narrow range of the parameters used here. The tested fractures are relatively smooth (JRC = 6-8), small (76×148 mm^2), and obtained from only one rock type.

10. Acknowledgements

This study is funded by Suranaree University of Technology and by the Higher Education Promotion and National Research University of Thailand. Permission to publish this paper is gratefully acknowledged.

References

[1] ASTM D5607-08, "Standard test method for performing laboratory direct shear strength tests of rock specimens under constant normal force" Annual Book of ASTM Standards 04.08, ASTM International, West Conshohocken, PA (2008).

[2] Brady B. H. G, and Brown E. T, Rock Mechanics for Underground Mining, Third Edition, Springer, Netherlands 2006.

[3] Jaeger J. C, Cook N. G. W. and, Zimmerman R. W, Fundamentals of Rock Mechanics, Fourth Edition, Blackwell Publishing, Oxford 2007.

[4] Barton N., "Shear strength investigations for surface mining" in: Proceedings of the 3rd International Conference on Surface mining, SME 1982, Vancouver pp 171-196.

[5] K. Fuenkajorn and N. Kenkhunthod, "Influence of loading rate on deformability and strength of three Thai sandstones," Geotechnical and Geological Engineering, 2010. Vol. 28, pp. 707-715.